ARTICLES
PUBLISHED ONLINE: 6 MARCH 2011 | DOI: 10.1038/NNANO.2011.24
nature nanotechnology

A high-throughput label-free nanoparticle analyser

Jean-Luc Fraikin[1], Tambet Teesalu[2], Christopher M. McKenney[1], Erkki Ruoslahti[2,3] and Andrew N. Cleland[1]*

Synthetic nanoparticles and genetically modified viruses are used in a range of applications, but high-throughput analytical tools for the physical characterization of these objects are needed. Here we present a microfluidic analyser that detects individual nanoparticles and characterizes complex, unlabelled nanoparticle suspensions. We demonstrate the detection, concentration analysis and sizing of individual synthetic nanoparticles in a multicomponent mixture with sufficient throughput to analyse 500,000 particles per second. We also report the rapid size and titre analysis of unlabelled bacteriophage T7 in both salt solution and mouse blood plasma, using just $\sim 1 \times 10^{-6}$ l of analyte. Unexpectedly, in the native blood plasma we discover a large background of naturally occurring nanoparticles with a power-law size distribution. The high-throughput detection capability, scalable fabrication and simple electronics of this instrument make it well suited for diverse applications.

Applications of synthetic nanoparticles include cosmetics[1], photovoltaics[2] and nanomedicine[3–5]. Naturally occurring microparticles and nanoparticles mediate important physiological processes[6–8], and lethal viruses with diameters of ~50–150 nm kill millions of people annually[9]. However, the practical development and use of nanoparticles is significantly constrained by a lack of practical tools capable of detecting and characterizing particles in this size range[10–12].

Size distributions are commonly extracted from bulk measurements such as dynamic light scattering (DLS) or disk centrifugation, which are inherently ensemble-averaging, limited in size resolution, and typically require relatively large ($\gtrsim 10^{-4}$ l) sample volumes. Individual nanoparticles can be studied by electron microscopy, but this approach is slow, expensive, and of little utility in assimilating large population statistics or detecting rare particles. Nanopores, coupled with electrical sensing such as the resistive pulse technique, provide a means to count and size individual nanoparticles. This approach, which is similar to the Coulter counter principle[13], has demonstrated good size resolution at the individual particle level[14–16], but cumbersome sensor fabrication[16,17] or low particle count rates[18,19] have prevented the practical adoption of such methods for characterizing nanoparticles.

Analyser operation

We have developed a nanoparticle analyser that combines a simply fabricated microfluidic design with a high-throughput electrical readout. The analyser has two components: a microfluidic channel, which directs the pressure-driven flow of analyte through the electrical sensor, carefully designed to maximize measurement bandwidth, and the sensor itself, comprising two voltage-bias electrodes and a single, optically lithographed readout electrode embedded in the microchannel (Fig. 1a). The analysis chips are simply fabricated at low cost, using single-layer optical lithography for electrode patterning, and well-established micromoulding techniques for defining the fluid channel that permit many chips to be made from a single mould (see Methods).

The fluid channel includes two main features: a primary nanoconstriction for particle detection, and a fluidic restriction that provides a balancing electrical resistance. Together, these components form a fluidic voltage divider that yields wide-bandwidth electrical detection of particles as they pass through the nanoconstriction (Fig. 1b,c). Constant voltages V_h and V_l (typically $\pm$1–3 V) are applied to the bias electrodes H and L respectively, generating an ionic electrical current in the analyte, with voltage drops across the fluidic resistor and the nanoconstriction (see Methods). The sensing electrode S is embedded in the channel between the fluidic resistor and the nanoconstriction. When a particle enters the constriction, it alters the ionic electrical current and, because of the voltage division between the fluidic resistor and the nanoconstriction, changes the electrical potential $V^\star$ of the fluid in contact with the sensing electrode. This potential change is capacitively coupled through the double-layer capacitance C_{DL} (ref. 20), changing the sensor electrode potential V_{out}. The signal is amplified with an operational amplifier a few millimetres from the sensing electrode. Although a variant of this fluidic resistor divider approach has been used previously to detect large particles with the resistive pulse technique (for diameters >1 μm; ref. 21), the device we present here is significantly simpler in design, capable of much more rapid detection rates (more than a factor of 10^4 higher), and can detect particles 100-fold smaller in diameter.

The signal generated by a single polystyrene particle with a diameter of 117 nm (Fig. 1d) demonstrates both the sensitivity and rapid electrical response of the sensor. The voltage signal ΔV_{out} scales as expected with particle diameter and bias voltage $V_h - V_l$ (Supplementary Fig. S1), and is proportional to the nanoparticle volume, allowing particle sizing (see Supplementary Information). Despite the rapid transit time of the particle (~10 μs), the detailed shape of the peak reflects both the geometric features of the nanoconstriction and the difference in fluid flow rates on opposite sides of the constriction. Under typical operating conditions, the fluid flow carrying particles away from the nanoconstriction on the downstream side is more rapid than the flow of incident particles, and leads to the asymmetric peak shape of the electrical signal. The sensor is able to respond to the short transient generated by the particle because of the minimal stray capacitance of the voltage divider and first-stage amplifier.

The flow of particles through the analyser is controlled by adjusting the fluid pressure at port P_5 on the downstream side of the nanoconstriction, determining whether particles pass into the waste

[1]Department of Physics, University of California Santa Barbara, California 93106, USA, [2]Vascular Mapping Laboratory, Center for Nanomedicine, Sanford-Burnham Medical Research Institute at University of California Santa Barbara, California 93106-9610, USA, [3]Cancer Research Center, Sanford-Burnham Medical Research Institute La Jolla, California 92037, USA. *e-mail: anc@physics.ucsb.edu

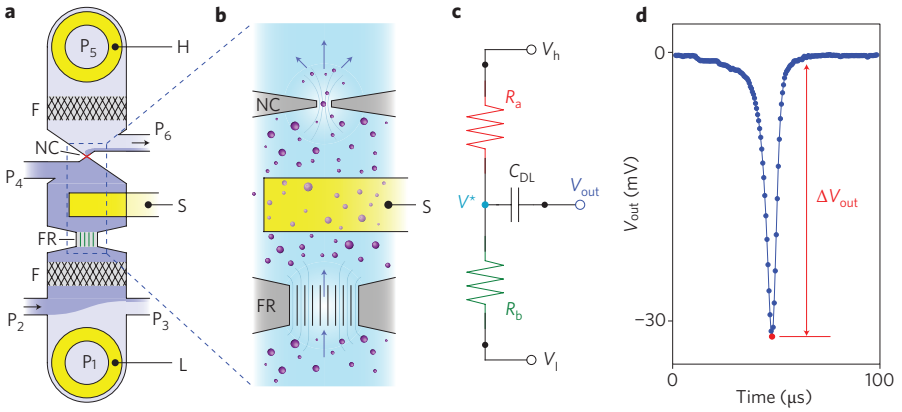

Figure 1 | Device schematics and detector response. a, Overall chip layout showing relative placement of the electrical and fluidic components of the device: external voltage bias electrodes (H, L) and sensing electrode (S); embedded nanometre-scale filters (F); fluid resistor (FR); nanoconstriction (NC); pressure-regulated fluidic ports (P_1–P_6). The nanoparticle suspension to be analysed (dark shading) enters the analyser at P_2 and exits at P_6, avoiding H and L. **b**, Detail of boxed area in **a**, showing the core sensing components. Nanoparticles in saline suspension flow in the direction of the arrows, and changes in the electrical potential of the fluid adjacent to the nanoconstriction are detected by the lithographed sensing electrode S. **c**, Electrical equivalent circuit: a constant bias voltage V_h (V_l) is applied to electrode H (L). Resistors R_a and R_b represent the electrical resistance of the nanoconstriction and the fluidic resistor, respectively. Electrode S is capacitively coupled to the fluid through the electric double-layer capacitance C_{DL}. Circuit elements R_a, R_b and C_{DL} are measured directly (see Supplementary Information). **d**, Output voltage V_{out} as a function of time as a single particle of nominal diameter 117 nm traverses the nanoconstriction, showing excellent time resolution and signal-to-noise ratio. The peak voltage change ΔV_{out} is proportional to $V_h - V_l$ and to the volume filling fraction of the particle in the nanoconstriction[40] (see Supplementary Information).

channel P_4 or through the nanoconstriction detection pathway (Fig. 2). We find that pressure-driven fluid flow is the dominant mechanism of mass transport in the system, with no significant contribution from electrokinetic or electroosmotic processes (Supplementary Fig. S2).

The high-throughput detection capability of the analyser is revealed by varying the particle flow rate (Fig. 3a). Each point in the figure indicates the measured relative diameter and transit time of an individual 117 nm particle, with data collected for >1,400 transits as the differential pressure across the nanoconstriction was varied between ~0.1 and 2 psi. Transit times as small as 2–3 μs per particle are easily resolved, more than two orders of magnitude faster than recent nanopore sensors[22,23]. Note that there is little increase in the spread of measured amplitudes as the transit time is reduced, yielding a good signal-to-noise ratio for even the most rapid transits. The full electrical bandwidth available for particle detection is obtained from the frequency dependence of the noise in V_{out} (Fig. 3b,c). We find a measurement bandwidth $f_{RC} \approx 650$ kHz, corresponding to a minimum sensor response time, $\tau_{min} \approx 750$ ns (see Methods). This implies a maximum particle count rate $1/2\tau_{min}$ exceeding 500,000 particles per second. A discussion of the effect of ionic strength on measurement bandwith is included in the Supplementary Information.

High-throughput multicomponent analysis

The concentration and size distribution of particles in a polydisperse mixture are highly relevant measures of manufactured or naturally occurring nanoparticles. We demonstrate the size resolution of this analyser and perform direct measurements of absolute particle concentrations using a mixture of synthetic nanoparticles with diameters from 40 to 130 nm. We compare the analyser results to those obtained using DLS, the most common technique for sizing particles below 1 μm.

A mixture containing particles with mean nominal diameters of 51 nm, 75 nm and 117 nm was prepared and analysed (see Methods). Three distinct signal amplitudes are visible in the output voltage time trace (Fig. 4a), corresponding to the three diameters in the population. The horizontal scale of the resulting histogram of particle diameters (Fig. 4b) was calibrated using the average voltage associated with the 117 nm particles. From this histogram, the two other particle sizes are found to correspond to mean diameters of 52 nm and 79 nm, with variances of 14% and 5.1%, respectively; these diameters and variances are in good agreement with the manufacturers' specifications.

When DLS was used to measure each of the monodisperse components separately, an application for which it is well suited (Fig. 4b; ref. 24), we found the measured diameters to agree to within 3% (see Methods). However, the nanosensor clearly outperforms DLS in resolving the subpopulation components of the polydisperse mixture, as is evident when the nanosensor histogram is compared to the corresponding DLS measurement results, in which the two smaller particle populations do not appear at all.

In addition to resolving polydispersity in a nanoparticle mixture, we can use the analyser to measure directly the absolute concentrations of the particles in the mixture. The fluid flow rate is calculated from the mean transit time of the 117 nm particles through the nanoconstriction (see Supplementary Information), and the number densities of the 50 nm, 75 nm and 117 nm particles in the mixture are found to be 1.8×10^9 ml^{-1}, 1.3×10^9 ml^{-1} and 3.6×10^9 ml^{-1}, respectively. The corresponding number densities calculated from the weight-percent of polystyrene in solution provided by the particle manufacturers are 2.8×10^9 ml^{-1}, 2.8×10^9 ml^{-1} and 3.0×10^9 ml^{-1}, respectively. The concentrations measured by the analyser differ by factors of ~0.5–1.2 from those calculated using the manufacturers' values; however, this factor remains constant for each size component even when varying the particle concentration by more than an order of magnitude (data not shown). The consistency and directness of the analyser approach suggest that, of the two methods, the nanosensor measurements probably lie closer to the true particle concentrations.

Rapid size and titre analysis of biological nanoparticles

The T7 bacteriophage is a bacterial virus commonly used for phage display of random peptides[25], and with a diameter of 55–65 nm it is comparable in size to non-enveloped small viruses such as Hepatitis C (~55 nm; ref. 26). After amplification, concentration and purification of the phage, its concentration in solution is usually determined by biological titre, a process that typically requires a few

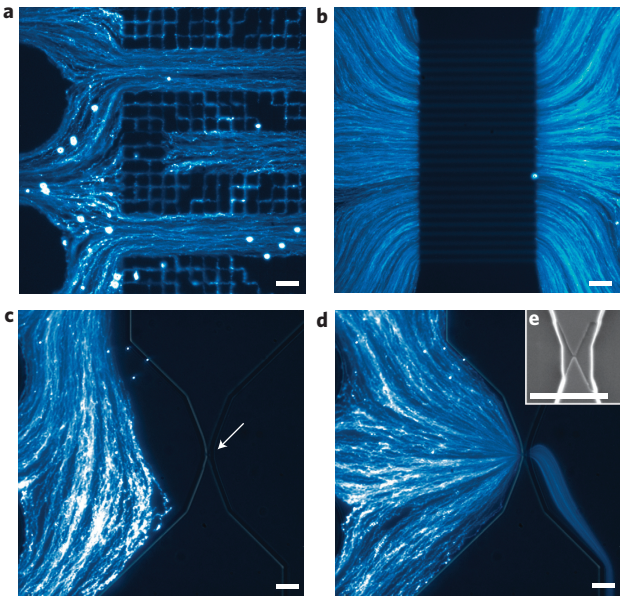

Figure 2 | Controlling particle flow. a–e, False-colour fluorescence micrographs (**a–d**) and scanning electron micrograph (**e**) showing the fluidic components of the analyser and control of particle flow. Fluorescent polystyrene nanoparticles (with diameters of ~200 nm) traverse the integrated nanofilter (**a**), and the fluidic electrical resistor (**b**) before reaching the vicinity of the nanoconstriction (indicated by the arrow in **c**). The black region in **b** is the sensing electrode. A single external pressure setting at port P_5 selects the flow path and flow rate of the fluid, sending particles either to the waste channel P_4 (**c**) or through the nanoconstriction (**d**). **e**, A representative PDMS nanoconstriction with lateral dimensions 250 × 250 nm^2, and depth 290 nm. Scale bars in all panels are 10 μm.

hours. As a first biological application of our detector, which highlights its high-throughput detection capabilities, we demonstrate the direct, rapid (few second) measurement of the size and concentration of T7 phage, an all-electronic analysis that does not require infectivity-based titration.

To calibrate the system, known dilutions of polystyrene nanoparticles with a diameter of 117 nm were added to a suspension of T7 phage in 1 M NaCl, and a 1 μl aliquot taken for analysis (see Methods). A representative 1 s measurement shows the detection of more than 125 phage virions (Fig. 5a). A 5 s accumulation yields the complete size distribution of the particles in the sample (Fig. 5b). By calibrating against the 117 nm particles, we measured the phage virion volume to be 144 × 10^3 nm^3, corresponding to an effective diameter of 65 nm (large peak in histogram). This diameter lies within the range of values measured for virions in a number of salt suspensions, using indirect methods such as buoyant density sedimentation and X-ray scattering[27–30]. The small-amplitude peak corresponding to an effective diameter of 81 nm is consistent with a small population of phage doublets, which are probably phage dimers (see Supplementary Information). DLS measurements of the pure phage sample yielded a single broad peak (Fig. 5b), emphasizing the finer resolution of the microfluidic analyser, with the ability to detect minority populations in a heterogeneous sample.

The concentration of phage was obtained by comparing the ratio of the phage count (~520) to that of 117 nm particles (~45), yielding 4.1 × 10^{10} virion per ml. This is in good agreement with the concentration of infective phage measured by biological titre, 2.3 × 10^{10} plaque forming units (pfu) per ml. The electronically measured concentration was obtained in 5 s of analysis, rather than the ~4 h required for biological titre (see Methods). Our concentration measurement, when combined with the results of live biological titre, provides a means to estimate the fraction of infective phage in the sample (~55% in this case).

Measurements of the viral load in blood are routinely used to monitor the severity of chronic viral infections such as HIV (~130 nm) and Hepatitis C (~55 nm). To validate the potential use of the analyser as a clinical tool for measuring viral load in blood, we analysed the distribution of naturally occurring nanoparticles in mouse blood plasma, and performed the same analysis with plasma spiked with T7 phage. We successfully detect the T7 phage in plasma, and obtain a measure of the viral concentration.

Two samples were prepared and analysed (see Methods). The first (phage-infected) sample consisted of mouse blood plasma to which polystyrene calibration particles (with a diameter of 117 nm) and T7 phage were added. In the second (control) sample, phosphate-buffered saline (PBS) was added in lieu of the phage suspension, while also including calibration particles. When the control mixture was analysed, the output signal and corresponding histogram (Fig. 6a,b) indicated the detection of the 117 nm

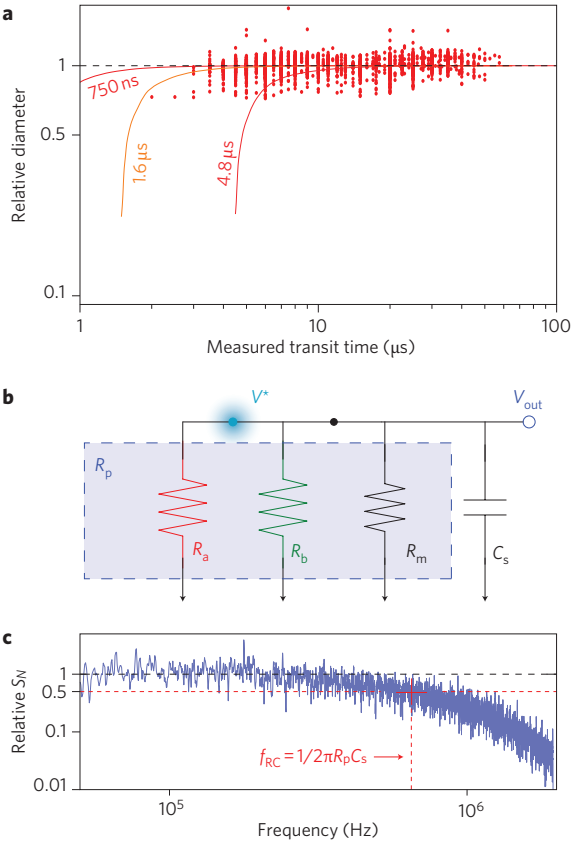

Figure 3 | Detection bandwidth. a, Measured relative particle diameter as a function of transit time (full width at half maximum) on a logarithmic scale as 117 nm nanoparticles pass through the nanoconstriction, using a range of flow rates, showing high-fidelity detection and sizing for single-particle transit times as small as 2 μs. Solid curves indicate the expected signal attenuation for three different minimum sensor response times. **b**, High-frequency equivalent circuit model of the sensor including the input resistance of the first-stage amplifier R_m and the stray capacitance C_s. R_p is the equivalent resistance of the parallel combination of the fluid resistances R_a and R_b with R_m. **c**, Spectral density S_N of the noise in V_{out} for zero voltage bias, normalized by the expected thermal Nyquist noise of the effective resistance R_p, from which we determine the detector electrical bandwidth $f_{RC} \equiv 1/2\pi R_p C_s \approx 650$ kHz. The spectrum was obtained by averaging ten Fourier transforms of V_{out} versus time.

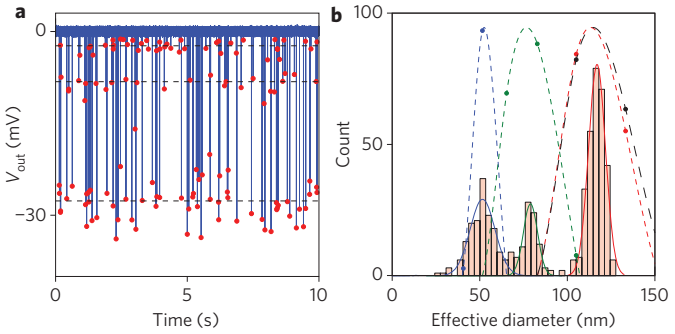

Figure 4 | Analysis of a polydisperse nanoparticle mixture. a, Output voltage V_{out} versus time for a mixture of nanoparticles of different diameter (51 nm, 75 nm and 117 nm). Events marked with red circles cluster around three values of V_{out} (horizontal dashed black lines). **b**, Histogram of effective diameters (40 s measurement). The 117 nm peak is used to calibrate the horizontal axis, relative to which the other peaks correspond to diameters of 52 nm and 79 nm. Separately normalized DLS measurements of each population are indicated by spline fits (dashed blue, green and red lines), as are measurements of the mixture (dashed black line). The scattering signal from the 117 nm particles dominates the DLS measurement of the mixture, and results in a nearly identical measurement to that of the pure 117 nm particle solution. Using the mean transit time of the 117 nm nanoparticles to estimate the fluid flow rate, we find the absolute number densities are within factors of ~0.5–1.2 of those calculated from the manufacturers' specifications (see main text).

calibration particles, and a large concentration of background nanoparticles. A detailed analysis of this trace (Supplementary Fig. 3) showed that particles as small as 46 nm in diameter could be resolved easily from noise, and that >70% of detected particles had an uncertainty in their measured diameter of less than 10%. Unexpectedly, we found that the concentration c of particles in this size range in the native plasma exhibited a striking power-law dependence on particle volume v_p, $c \propto v_p^{-3.3}$ (Fig. 6c). This is unlikely to result from random coincidences of pairs or groups of smaller particles: even the highest measured concentration is three orders of magnitude below that for which the average solution volume per particle equals the sensing volume. We discuss the significance of this measurement in more detail below.

Both representative 1 s time traces of V_{out} (Fig. 6a,d) and the corresponding diametric histograms (Fig. 6b,e) indicate background particles with diameters $\lesssim$60 nm. When the number density distributions from the two plasma samples are compared (Fig. 6f), a clear peak due to the phage is visible. The position of the peak yields the measured diameter of the phage, ~55 nm relative to the calibration particles. This diameter is slightly smaller than that measured in 1 M NaCl (~65 nm, Fig. 5b), but lies within the range of published values[27–30]. The difference in the measurements may reflect changes in the mean capsid diameter in solutions of differing osmotic strength. Integration of the number density of the infected sample, while subtracting the background particles, yields the concentration of T7 phage in the plasma, 5.3×10^{10} ml^{-1}. This value is close to that obtained by biological titre, 1.5×10^{10} pfu ml^{-1}, and suggests a slightly lower infective fraction in this batch of phage (~30%). Comparison of the infective fractions from biological titre and quantitative PCR-based copy number determination indicates that in a typical phage preparation, the infective fraction can be as low as 20% (T. Teesalu *et al.*, unpublished observations).

The detection of virus in blood using a similar size-based assay will be limited by the background concentration of naturally occurring nanoparticles. From our measurements (Fig. 6c), we calculated a detection limit in the unprocessed plasma of $\sim 1 \times 10^8$ ml^{-1} for virions with diameters of 55 ± 3 nm (signal-to-background ratio of unity), comparable to but an order of magnitude higher than typical clinical viral loads reported for Hepatitis C ($\sim 1 \times 10^7$ ml^{-1}; ref. 31).

Outlook

We have developed a simple microfluidic analyser that permits rapid electronic detection and volumetric analysis of unlabelled nanoparticles, including virus suspended in salt solution and in blood plasma. The device design enables the detection of individual nanoparticles with good signal-to-noise ratio at high count rates. The low-cost, scalable fabrication method, as well as the simple readout electronics, make this analyser potentially useful in a wide range of applications.

Measurements of blood plasma using the analyser reveal a large background of naturally occurring nanoparticles (Fig. 6a–c), with a concentration c that follows a power-law dependence on particle volume v_p ($c \propto v_p^{-3.3}$). These background particles probably include cell-derived vesicles such as exosomes, which are known to be present in blood plasma and are implicated in a variety of physiological and pathological processes[7,8,32]. Previous studies of these particles have required extensive sample preparation and purification, with particle sizes typically analysed by electron microscopy. The measurements we present here are, to our knowledge, the first analyses of the size distributions of these particles in their native state. The microfluidic analyser performs these measurements with little sample preparation, and yields a moderate sample size ($>1 \times 10^4$ particles for the data in Fig. 6c) with data accumulated in only ~10 s. The analyser may prove a useful tool for systematic physiological and disease studies of plasma exosomes and other nanoparticles.

The high background of plasma-borne nanoparticles with diameters less than ~100 nm makes viral detection in plasma challenging. It may be possible to increase the sensitivity of the assay by reduction of the background through further sample preparation (for example, removal of background nanoparicles by detergent exposure) or by the addition of affinity reagents (for example by increasing the apparent size of target virus particles, or by forming aggregates), routes that we have not explored here.

Moreover, the range of nanoparticle diameters that can be analysed using this approach can be significantly increased beyond

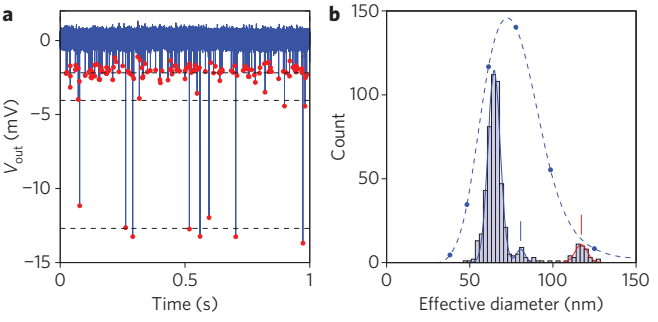

Figure 5 | Size and concentration measurements of unlabelled bacteriophage T7 in salt solution. a, Output voltage V_{out} versus time for a 1 s measurement, showing direct detection of unlabelled bacteriophage T7 virions (~65 nm), with an admixture of 117 nm calibration particles. Events cluster around three values of V_{out} (horizontal dashed lines). **b**, Histogram of effective diameters displaying two phage particle diameters (blue outline), in addition to the calibration particles (red outline). Outlines are Gaussian least-square fits. The mean effective diameters are 65 nm, which corresponds to T7 virion singlets, and 81 nm, an effective diameter corresponding to virion dimers, with ~10% of phage apparently in dimer form. A normalized DLS measurement of the pure phage sample (no calibration particles) is indicated by a spline fit (blue points and dashed line).

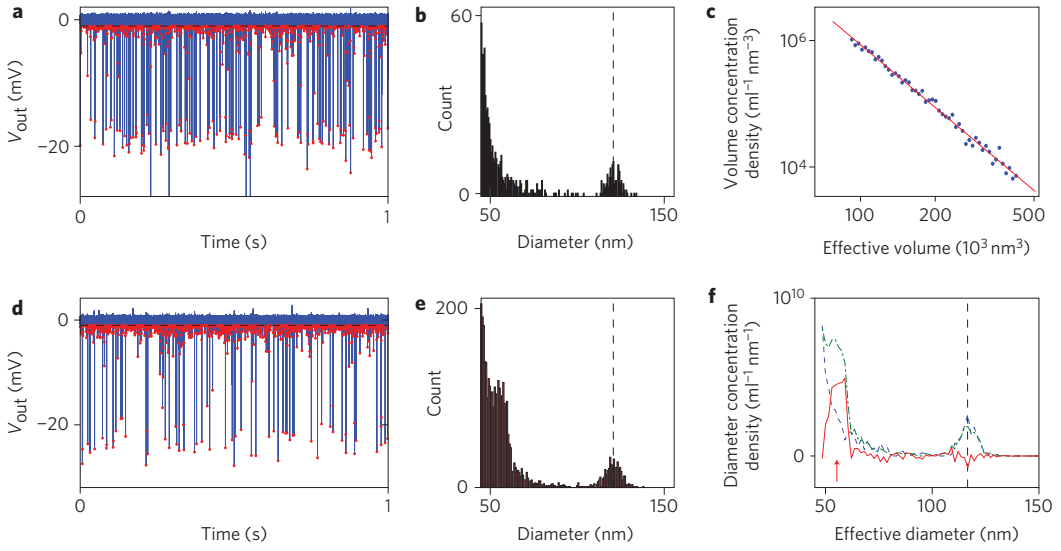

Figure 6 | Particle size distribution and T7 phage detection in mouse blood. a, Representative 1 s time trace of V_{out} while sampling mouse blood plasma with an admixture of calibration particles (diameter, 117 nm; control); trace shows detection of $\gtrsim$1,300 particles. **b**, Histogram of particle diameters obtained from the trace in **a**, showing large numbers of particles at small diameters ($\lesssim$60 nm). **c**, Particle concentration as a function of particle volume for diameters from ~50 nm to 100 nm. The fit shown by the red line indicates the power-law dependence of concentration c on particle volume v_p, with $c \propto v_p^{-3.3}$. **d**, Output voltage V_{out} versus time while sampling T7 phage-infected plasma. **e**, Histogram of effective particle diameters, showing a peak in particle concentration at ~55 nm attributed to phage. **f**, Number density distributions of the blank plasma (blue dashed), phage-infected plasma (green dot-dashed) and the difference (red solid). The position of the peak (red arrow) in the difference curve yields the measured diameter of the phage to be 55 nm. Integration of the peak gives the measured phage concentration of 5.3×10^{10} particles per ml, near that obtained by biological titre (1.5×10^{10} pfu ml^{-1}).

the narrow range demonstrated with this one-channel design. A multichannel design can easily be configured (with little increase in fabrication or measurement complexity) to allow the analysis of sizes ranging by over 1 to 2 orders of magnitude; this can be achieved by making parallel analyser channels in which the size of the nanoconstriction and its fluidic filter are systematically varied. A single inexpensive disposable chip could then rapidly size particles with diameters ranging from 10 nm to a few micrometres.

The high-throughput capabilities of the detector are well suited for the detection of rare particles. For example, TiO_2 nanoparticles have been observed in the tertiary effluent of wastewater treatment plants, with titanium concentrations of ~10 μg ml^{-1} (refs 33,34). For 100-nm-diameter particles, this concentration would imply a number density of ~1×10^6 particles per ml. At this concentration, the detection rates possible with previous nanoparticle detectors[18] would require more than five days to sample sufficient fluid to detect ~100 particles, whereas the analyser described here could achieve the same in about 20 min.

Methods

Device fabrication and assembly. The microfluidic channel was made of poly(dimethylsiloxane) (PDMS) using well-established micromoulding techniques, sealed to a glass chip onto which the gold readout electrode had been patterned[35–39] (see Supplementary Information). Detailed descriptions of the fabrication of the micromould and sensing electrodes, as well as the final assembly of the analyser chips, are included in the Supplementary Information.

Electrical operation. Constant voltages V_h and V_l (typically a few volts in amplitude) were applied at bias electrodes H and L respectively (Fig. 1a), using two Keithley 2400 source meters operating in voltage-source mode. The bias voltages were set to keep the average difference $|V^\star - V_{out}|$ near zero, eliminating electrolytic corrosion of the sensing electrode. A model for the dynamic electrical response of the analyser is included in the Supplementary Information.

Detection bandwidth. The fluidic voltage divider implemented here affords a larger detection bandwidth than earlier nanoparticle resistive pulse sensors (see Supplementary Information for discussion). According to the high-frequency electrical model of the sensor (Fig. 3b), the minimum time required for a 95% response in V_{out} from a change in $V^\star$ is $\tau_{min} = 3R_pC_s$. Attenuation will occur for signals from particles passing through the sensor in times less than $2\tau_{min}$, or fluctuations in $V^\star$ at frequencies $f > f_{RC} \equiv 1/2\pi R_pC_s$. We measured f_{RC} using the noise in V_{out} at zero bias: as white thermal noise from the fluidic resistors dominates, the frequency of the 3 dB roll-off point in noise corresponds to the measurement bandwidth (Fig. 3c). We find $f_{RC} \approx 650$ kHz, from which we obtain $\tau_{min} \approx 750$ ns. This response time implies a maximum achievable detection rate exceeding 500,000 particles per second. The effect of ionic strength on measurement bandwidth is discussed in the Supplementary Information.

Peak analysis. Custom software was written for a Matlab environment (The Mathworks, Inc.) to recognize and measure peaks in V_{out}. After minimal filtering of the raw data, each voltage minimum exceeding a particular threshold was measured relative to a local baseline, and peak widths were measured at half-maximum (see Supplementary Information).

Polystyrene nanoparticle preparation. Fluorescent polystyrene nanoparticles were obtained from Polysciences Inc. (117 nm, catalogue no. 16662) and from Thermo Scientific (51 nm and 75 nm; G51 and G75, respectively). Number densities in stock solution were calculated from manufacturers' specifications, and the particles were diluted as needed (typical final concentration ~1×10^9 ml^{-1}) into 1 M NaCl with 1% Tween 20 (Sigma). For the plasma mixtures, 117 nm calibration particles were suspended in 10× PBS with 5% Tween 20 at least 1 day before use, to prevent agglomeration in the plasma.

Dynamic light scattering. A DynaPro Nanostar (Wyatt Technology Corporation) was used for all DLS measurements. A standard disposable cuvette was used to hold ~100 μl of the suspension to be analysed. Multiple measurements of each sample were averaged to improve accuracy. The heights of the peaks in the DLS data (Figs 4b, 5b) are normalized for clarity. The polystyrene nanoparticles with nominal diameters 51 nm and 75 nm (as specified by the manufacturer) were measured with DLS to have mean diameters of 51 nm and 77 nm, respectively.

T7 phage preparation. T7 bacteriophage was prepared according to ref. 25. Briefly, the phage was cloned according to the manufacturer's instructions using the T7-select phage display system (EMD Biosciences). It was then purified by precipitation with PEG-8000 (Sigma), purified with $CsCl_2$ gradient ultracentrifugation, and dialysed into 1× PBS.

T7 phage concentration by biological titre. *Escherichia coli* BLT5615 cells (OD600-0.5; 600 μl) were mixed with a serial dilution of the concentrated phage suspension and plated on Lysogeny Broth-Agar petri dishes. After 4 h at 37 °C, the plaques in the bacterial layer were counted to estimate the concentration of infectious phage.

Mouse blood plasma preparation. Approximately 8 μl of whole blood was extracted from a healthy mouse by pricking the tail vein. Ethylenediaminetetraacetic

acid (EDTA) was added immediately to prevent clotting. Large particles and cells were separated from the plasma by centrifugation at 400*g* for 5 min. The T7 plasma sample was composed of plasma diluted to 0.4× its original concentration in ~5× PBS with 2% Tween 20, 117 nm calibration particles, and T7 bacteriophage. In the control plasma sample, an equal volume of 1× PBS with 5% Tween 20 replaced the phage suspension.

Received 17 December 2010; accepted 4 February 2011; published online 6 March 2011

References

1. Nohynek, G. J., Lademann, J., Ribaud, C. & Roberts, M. S. Grey goo on the skin? Nanotechnology, cosmetic and sunscreen safety. *Crit. Rev. Toxicol* **37,** 251–277 (2007).
2. Franzman, M. A., Schlenker, C. W., Thompson, M. E. & Brutchey, R. L. Solution-phase synthesis of SnSe nanocrystals for use in solar cells. *J. Am. Chem. Soc.* **132,** 4060–4061 (2010).
3. Sugahara, K. N. *et al.* Tissue-penetrating delivery of compounds and nanoparticles into tumors. *Cancer Cell* **16,** 510–520 (2009).
4. Michalet, X. *et al.* Quantum dots for live cells, *in vivo* imaging, and diagnostics. *Science* **307,** 538–544 (2005).
5. Harisinghani, M. G. *et al.* Noninvasive detection of clinically occult lymph-node metastases in prostate cancer. *New Engl. J. Med.* **348,** 2491–2499 (2003).
6. VanWijk, M. J., VanBavel, E., Sturk, A. & Nieuwland, R. Microparticles in cardiovascular diseases. *Cardiovasc. Res.* **59,** 277–287 (2003).
7. Valadi, H. *et al.* Exosome-mediated transfer of mRNAs and microRNAs is a novel mechanism of genetic exchange between cells. *Nature Cell. Biol.* **9,** 654–659 (2007).
8. Simons, M. & Raposo, G. Exosomes—vesicular carriers for intercellular communication. *Curr. Opin. Cell Biol.* **21,** 575–581 (2009).
9. WHO. *World Health Statistics 2010* (WHO, 2010).
10. Cressey, D. Tiny traits cause big headaches. *Nature* **467,** 264–265 (2010).
11. Nel, A., Xia, T., Madler, L. & Li, N. Toxic potential of materials at the nanolevel. *Science* **311,** 622–627 (2006).
12. Maynard, A. D. *et al.* Safe handling of nanotechnology. *Nature* **444,** 267–269 (2006).
13. Coulter, W. H. Means for counting particles suspended in a fluid. US patent 2,656,508 (1953).
14. DeBlois, R. W. & Bean, C. P. Counting and sizing of submicron particles by the resistive pulse technique. *Rev. Sci. Instrum.* **41,** 909–916 (1970).
15. Kasianowicz, J. J., Brandin, E., Branton, D. & Deamer, D. W. Characterization of individual polynucleotide molecules using a membrane channel. *Proc. Natl Acad. Sci. USA* **93,** 13770–13773 (1996).
16. Li, J., Gershow, M., Stein, D., Brandin, E. & Golovchenko, J. A. DNA molecules and configurations in a solid-state nanopore microscope. *Nature Mater.* **2,** 611–615 (2003).
17. Uram, J. D., Ke, K., Hunt, A. J. & Mayer, M. Label-free affinity assays by rapid detection of immune complexes in submicrometer pores. *Angew. Chem. Int. Ed.* **45,** 2281–2285 (2006).
18. Saleh, O. A. & Sohn, L. L. An artificial nanopore for molecular sensing. *Nano Lett.* **3,** 37–38 (2003).
19. Sen, Y-H. & Karnik, R. Investigating the translocation of λ-DNA molecules through PDMS nanopores. *Anal. Bioanal. Chem.* **394,** 437–446 (2009).
20. Bard, A. J. *Electrochemical Methods Fundamentals and Applications* 2nd edn (Wiley, 1980).
21. Sridhar, M. *et al.* Experimental characterization of a metal-oxide-semiconductor field-effect transistor-based coulter counter. *J. Appl. Phys.* **103,** 104701 (2008).
22. Uram, J. D., Ke, K., Hunt, A. J. & Mayer, M. Submicrometer pore-based characterization and quantification of antibody–virus interactions. *Small* **2,** 967–972 (2006).
23. Saleh, O. A. & Sohn, L. L. Quantitative sensing of nanoscale colloids using a microchip Coulter counter. *Rev. Sci. Instrum.* **72,** 4449–4451 (2001).
24. Berne, B. J. *Dynamic Light Scattering: With Applications to Chemistry, Biology, and Physics* (Wiley, 1976).
25. Teesalu, T., Sugahara, K. N., Kotamraju, V. R. & Ruoslahti, E. C-end rule peptides mediate neuropilin-1-dependent cell, vascular, and tissue penetration. *Proc. Natl Acad. Sci. USA* **106,** 16157–16162 (2009).
26. Wakita, T. *et al.* Production of infectious hepatitis C virus in tissue culture from a cloned viral genome. *Nature Med.* **11,** 791–796 (2005).
27. Davison, P. F. & Freifelder, D. The physical properties of T7 bacteriophage. *J. Mol. Biol.* **5,** 635–642, IN2 (1962).
28. Ronto, G., Agamalyan, M. M., Drabkin, G. M., Feigin, L. A. & Lvov, Y. M. Structure of bacteriophage-T7—small-angle X-ray and neutron-scattering study. *Biophys. J.* **43,** 309–314 (1983).
29. Serwer, P. Buoyant density sedimentation of macromolecules in sodium iothalamate density gradients. *J. Mol. Biol.* **92,** 433–448 (1975).
30. Stroud, R. M., Serwer, P. & Ross, M. J. Assembly of bacteriophage-T7—dimensions of the bacteriophage and its capsids. *Biophys. J.* **36,** 743–757 (1981).
31. Berg, T. *et al.* Prediction of treatment outcome in patients with chronic hepatitis C: significance of baseline parameters and viral dynamics during therapy. *Hepatology* **37,** 600–609 (2003).
32. Caby, M-P., Lankar, D., Vincendeau-Scherrer, C., Raposo, G. & Bonnerot, C. Exosomal-like vesicles are present in human blood plasma. *Int. Immunol.* **17,** 879–887 (2005).
33. Kiser, M. A. *et al.* Titanium nanomaterial removal and release from wastewater treatment plants. *Environ. Sci. Technol.* **43,** 6757–6763 (2009).
34. Gottschalk, F., Sonderer, T., Scholz, R. W. & Nowack, B. Modeled environmental concentrations of engineered nanomaterials (TiO_2, ZnO, Ag, CNT, fullerenes) for different regions. *Environ. Sci. Technol.* **43,** 9216–9222 (2009).
35. Duffy, D., McDonald, J., Schueller, O. & Whitesides, G. Rapid prototyping of microfluidic systems in poly(dimethylsiloxane). *Anal. Chem.* **70,** 4974–4984 (1998).
36. Fraikin, J-L., Requa, M. V. & Cleland, A. N. Probing the Debye layer: capacitance and potential of zero charge measured using a Debye-layer transistor. *Phys. Rev. Lett.* **102,** 156601 (2009).
37. Wood, D. K., Oh, S-H., Lee, S-H., Soh, H. T. & Cleland, A. N. High-bandwidth radio frequency Coulter counter. *Appl. Phys. Lett.* **87,** 184106 (2005).
38. Wood, D. K., Requa, M. V. & Cleland, A. N. Microfabricated high-throughput electronic particle detector. *Rev. Sci. Instrum.* **78,** 104301 (2007).
39. Wood, D. K. *et al.* A feasible approach to all-electronic digital labeling and readout for cell identification. *Lab Chip* **7,** 469–474 (2007).
40. Kubitscheck, H. E. *Counting and Sizing Micro-organisms with the Coulter Counter* Vol. 1, Ch. XXVII, 593–610 (Academic, 1969).

Acknowledgements

This research was supported by a National Institutes of Health Program of Excellence in Nanotechnology grant (U01-HL080718). The authors thank C. Axline for construction of the pressure manifold used to control flow in the microfluidic system, and G. Braun for valuable discussions. The authors also acknowledge use of the UC Santa Barbara Nanofabrication Facility, a part of the NSF-supported National Nanofabrication Infrastructure Network (NNIN).

Author contributions

J.-L.F. fabricated the analyser, performed the experiments and analysed the data. J.-L.F. and A.N.C designed the analyser. J.-L.F., T.T. and A.N.C. designed the experiments with contributions from E.R. J.-L.F. and A.N.C. wrote the manuscript with contributions from T.T. T.T. performed the biological procedures, including phage synthesis. C.M.M. contributed to the fabrication of the fluidic mold.

Additional information

The authors declare no competing financial interests. Supplementary information accompanies this paper at www.nature.com/naturenanotechnology. Reprints and permission information is available online at http://npg.nature.com/reprintsandpermissions/. Correspondence and requests for materials should be addressed to A.N.C.